Semiconductor-metal transition in liquid As-Te mixtures

2000 J. Phys.: Condens. Matter 12 6077

(http://iopscience.iop.org/0953-8984/12/28/306)

J. Phys.: Condens. Matter **12** (2000) 6077–6099. Printed in the UK PII: S0953-8984(00)11731-X

Semiconductor–metal transition in liquid As–Te mixtures

H Endo†, H Hoshino‡, H Ikemoto†§ and T Miyanaga†‖

† Faculty of Engineering, Fukui University of Technology, Fukui 910-8505, Japan
‡ Faculty of Education, Hirosaki University, Hirosaki, Aomori 036-8560, Japan
§ Faculty of Science, Toyama University, Toyama 930-8555, Japan
‖ Faculty of Science and Technology, Hirosaki University, Hirosaki, Aomori 036-8561, Japan

Received 9 February 2000, in final form 28 April 2000

Abstract. EXAFS, conductivity and Hall coefficient measurements have been carried out for liquid As–Te mixtures. EXAFS analysis reveals the presence of chemical disorder marked by the existence of homopolar As–As and Te–Te pairs. At high temperature around 500 °C the network structure composed of threefold coordinated As atoms and twofold coordinated Te atoms is transformed into the twofold chain structure. The network–chain transformation is accompanied by the gradual semiconductor to metal transition which is demonstrated by the results for conductivity and Hall coefficient. The microscopic origin of the semiconductor to metal transition is discussed in connection with the structural modification.

1. Introduction

The As chalcogenide glasses, especially the S and Se based glasses, have been extensively studied [1], while their liquids have been much less investigated. In recent years liquid As chalcogenides have attracted considerable interest, because it was found that the liquids undergo the semiconductor to metal (S–M) transition at high temperatures, being accompanied by structural transformation [2–5]. A similar electronic transition is observed for liquid Te–Se mixtures with twofold covalently bonded chain structure, of which the microscopic mechanism remains unsolved [6].

The crystalline $As_{40}Se_{60}$ has the orpiment layer structure [7]. The dominant structural unit is an –As–Se–As–Se– spiral chain; the remaining Se atoms are used to cross-link parallel chains. The structure is contrasted with that of Se, which consists of parallel spiral chains with no cross-linking atoms. The crystallographic data for $As_{40}Te_{60}$ by Carron [8] indicate that all Te atoms of the crystalline $As_{40}Te_{60}$ are threefold coordinated, whereas the As atoms are either in trigonal pyramid coordinated sites or octahedrally coordinated sites. The crystal consists of As_4Te_6 molecules which have a double chain structure in each molecule with weak bonds between molecules.

The structure of the glassy $As_{40}Se_{60}$ (g-$As_{40}Se_{60}$) can be considered to be a modified network of covalently linked $AsSe_{3/2}$ groupings [7]. The atomic arrangement of the crystalline $As_{40}Te_{60}$ (c-$As_{40}Te_{60}$) is not maintained in the glassy state. Ma *et al* [9] studied the local structure of g-As_xTe_{100-x} mixtures by extended x-ray absorption fine structure (EXAFS) and x-ray anomalous scattering. Their main achievements are summarized as follows. (a) Te atoms are twofold coordinated in As-rich mixtures ($x > 40$ at.% As), while the Te coordination suddenly increases to 2.4 at the stoichiometric $As_{40}Te_{60}$ composition, which indicates a large fraction of threefold Te sites in the glass. This percentage of occupancy of threefold Te

0953-8984/00/286077+23$30.00

sites remains almost constant with further increase of the Te concentration; (b) a significant level of chemical disorder, marked by the existence of homopolar As–As and Te–Te pairs in the first coordination shell, is observed for all the investigated glasses. Cornet and Rossier [10] suggested that for As-rich glasses ($x > 40$ at.% As) an additional As site emerges as x increases, which has one As and two Te neighbours. The short strong covalent As–As bond is considered as a pair lock stabilizing the glassy structure.

The structural study for liquid $As_{40}Te_{60}$ (l-$As_{40}Te_{60}$) was carried out using the neutron diffraction technique by Uemura *et al* [11]. They reported that the structure factor $S(Q)$ and radial distribution function $g(r)$ for l-$As_{40}Te_{60}$ are similar to those in the glassy state but not in the crystalline state. They did not observe any difference in the nearest neighbour distance and the coordination number between l-$As_{40}Te_{60}$ at 424 °C and l-$As_{40}Te_{60}$ at 625 °C. The difficulty of the analysis of the diffraction data lies in the fact that it is almost impossible to separate the partial structure factors from the total structure factor $S(Q)$. This difficulty is because the neutron scattering lengths of the two atoms in l-$As_{40}Te_{60}$ are not very different. The EXAFS spectra for l-$As_{40}Te_{60}$ around the As K edge in the temperature range up to 900 °C have been measured by Hosokawa *et al* [12]. They proposed that there exist As neighbours together with Te atoms around As atoms.

Recently x-ray diffraction [3], EXAFS [4], density [3], conductivity [5] and optical absorption [13] measurements for l-$As_{40}Se_{60}$ have been carried out. The diffraction pattern of l-$As_{40}Se_{60}$ contains a first sharp diffraction peak (FSDP) in $S(Q)$, which gives evidence for the medium range order. The FSDP disappears around 1000 °C, where the optical gap deduced from the absorption spectra closes. The S–M transition in l-$As_{40}Se_{60}$ is related to a substantial change of the short range atomic arrangement, which accounts for the anomalous behaviour around 1000 °C in the magnitude of the Fourier transform of the EXAFS spectra [4]. To understand the microscopic mechanism of the S–M transition in l-$As_{40}Se_{60}$, Shimojo *et al* [14] studied the structural and electronic properties of l-$As_{40}Se_{60}$ by means of *ab initio* molecular-dynamic simulations. Their simulation result shows that a major part of the l-$As_{40}Se_{60}$ near the S–M transition region [4] consists of twofold chainlike structure, which is similar to our observation for l-As_xTe_{100-x} mixtures at high temperature [2, 15].

Liquid Te exhibits metallic behaviour near the triple point and the transition to the semiconducting state occurs in the supercooled liquid state. Dating back to the early diffraction experiments [16], there has been a tendency to interpret the radial distribution data for metallic l-Te in terms of a transition to threefold coordination. But a recent re-examination of the data by Enderby and Barnes [17] has led them to conclude that the twofold covalent bonding persists, though there is substantial penetration of the first coordination sphere by noncovalently bonded atoms. Kawakita *et al* [18] have analysed carefully the EXAFS spectrum for l-Te by adopting a model independent method. They found that the shortened twofold chains in l-Te with metallic character are composed of short and long covalent bonds and that the long bonds vanish in the semiconducting state. Much of the interest in l-Te stems from the apparent persistence of twofold covalent bonding across the S–M transition. The thermopower remains positive across the S–M transition [19]. The presence of shortened chains with broken bonds induces a nondirectional bonding interaction between neighbouring twofold bonded molecules. Recently Endo and co-workers [2, 18, 20] have proposed that this bonding interaction could cause large fluctuations of charge distribution within the shortened chains.

The purpose of the present paper is to discuss what characterizes the bonding configurations on the S–M transition in l-As_xTe_{100-x} mixtures. The EXAFS technique is complementary to the diffraction experiments, since it can provide selective information concerning the local structure of liquid mixtures. The Hall coefficient measurement is a good means of understanding the microscopic transport, since it depends on the conduction

affected by the topological geometry of atoms. EXAFS, dc conductivity and Hall coefficient measurements have been carried out for l-As_xTe_{100-x} mixtures. From EXAFS data we deduce the modification of local structures around As and Te atoms near the S–M transition region.

2. Experiment

2.1. Sample preparation

The As–Te mixtures were prepared by heating weighed amounts of As and Te, which were sealed in a quartz ampoule (inner diameter 8 mm) under a vacuum of 10^{-6} Torr. The purities of As and Te were 99.9999% and 99.999%, respectively. After mixing at 800 °C for 24 hours the ampoule was cooled down to room temperature in air. A glassy sample with the stoichiometric $As_{40}Te_{60}$ composition cannot be prepared by quenching with slow cooling rate. Therefore the g-$As_{40}Te_{60}$ mixtures were prepared by quenching the quartz ampoule (inner diameter 2 mm), which contains the melt kept around 800 °C, in cold water. It was checked to be glassy by differential thermal analysis [21]. In our previous paper [22] it was reported that a Te droplet with an average diameter of 20 nm confined in an NaCl mixture was supercooled down to 240 °C, i.e. 210 °C below the melting point. The As chalcogenide fine particles (∼100 nm) dispersed and isolated in an NaCl matrix were used for some of the EXAFS samples in order to obtain the data in a wide temperature range including the supercooled liquid state below the melting point.

2.2. EXAFS

As and Te K-edge x-ray absorption spectra for the mixtures were obtained at BL 10B of the Photon Factory (PF) at KEK (Tsukuba). A typical photon flux was 10^9 photons s^{-1} with an electron beam energy of 3.0 GeV and a stored ring current of 300 mA. A Si(311) channel-cut crystal monochromator was used. X-ray absorption spectra were recorded in transmission mode using the ionisation chamber detector. The lengths of the ionisation chambers are 170 mm and 310 mm, and the gases in the chambers are Ar and Kr for front (I_0) and rear (I) detector of the sample, respectively. The samples were put in a quartz cell with appropriate length (e.g. 90 μm for $As_{40}Te_{60}$). The edge jumps were about 1.0–1.5. The EXAFS interference function, $\chi(k)$, was extracted from the absorption spectra and was Fourier transformed by the XANADU code described elsewhere [23]. The analysis procedure is given only briefly here. The normalized EXAFS interference function, $\chi(k)$, is expressed as

$$\chi(k) = \frac{\mu(k) - \mu_b(k) - \mu_0(k)}{\mu_0(k)} \tag{1}$$

$$k = \sqrt{\frac{2m}{\hbar^2}(E - E_0)} \tag{2}$$

where k is the photoelectron wavenumber, m is the mass of the electron, E is the energy of the incident x-ray and E_0 is the threshold energy which is tentatively determined to be the mid-point of the edge jump. $\mu(k)$ is the total absorption coefficient, $\mu_0(k)$ is the absorption due only to K-shell excitation of the central atom and $\mu_b(k)$ is the background contribution to $\mu(k)$ from the other shells. $\mu_b(k)$ was calculated by a least-squares fitting calculation with a formula, $aE^{-3} - bE^{-4} - c$, which comprises Victoreen's formula and a constant c. $\chi(k)$ was multiplied by a Hamming window function to reduce the ripples in the Fourier-transformed spectra in r-space. The k-range for the Fourier transform is from 3 to 12 $Å^{-1}$.

The Fourier peak of interest was filtered by multiplying by a similar window function and was inverse Fourier transformed into k-space again. The ranges of the inverse Fourier

transforms were about 2–4 Å including main peaks. In order to obtain the structural parameter of the interatomic distance, the coordination number and Debye–Waller factor, the EXAFS function was fitted by a non-linear least-squares method to the theoretical function as

$$\chi(k) = \sum_j \frac{BN_j}{k_j r_j^2} f_j(k_j, r_j) \exp(-2\sigma_j^2 k_j^2) \exp\left(-\frac{2r_j}{\lambda(k_j)}\right) \sin[2k_j r_j + \phi_j(k_j)] \tag{3}$$

where r_j is the interatomic distance between x-ray absorbing and photoelectron scattering atoms in the jth shell and N_j is the coordination number of the jth shell. $f_j(k_j, r_j)$ and $\phi_j(k_j)$ are the backscattering amplitude and the total phase shift functions for an atom in the jth shell, which are calculated by the FEFF6 code [24]. $\lambda(k_j)$ is the electron mean free path for an atom in the jth shell, which is calculated by the FEFF6 code [24]. σ^2 is the mean square displacement.

The photoelectron wave number k_j for the jth shell is a function of

$$k_j = \sqrt{k^2 - \frac{2m}{\hbar^2}\Delta E_{0j}}. \tag{4}$$

ΔE_0 were determined from standard samples of As and Te as 5.9 eV for the As K edge and 10.44 eV for the Te K edge. $B = AS_0^2(k)$. $S_0^2(k)$ is the k-dependent reduction factor due to the many body effect and obtained from FEFF6. A is a constant factor which is determined from the standard samples. Fourier filtering was performed for the main peak including two contributions, As–As and As–Te for the As K edge, or Te–As and Te–Te for the Te K edge.

The index of fit is a residual, R, calculated by

$$R = \sqrt{\frac{\sum k^6(\chi - \chi_{\text{cal}})^2}{\sum k^6 \chi^2}} \tag{5}$$

where χ is the EXAFS signal and the summation is taken over all the data points in the k-range used for fitting. In the present study, R is approximately 5–20%.

It is noticed that EXAFS for l-chalcogens and l-chalcogenides gives mainly information on the local arrangements of neighbouring covalently bonded atoms and the atomic correlation between adjacent chains which are weakly bonded is substantially smeared out by large fluctuations of bonding distance. Therefore, the above EXAFS analysis is considered to be reasonable in spite of the limitation of the model.

2.3. Dc conductivity

The dc conductivity σ_{dc} of the liquid As_xTe_{100-x} mixtures has been measured by means of the dc four probe method. The pressure was realized in an internally heated autoclave. Argon gas was employed as a pressure medium.

2.4. Hall coefficient

A quartz cell for the measurement of Hall coefficients consists of a tube and two polished discs. The upper one consists of a sample reservoir and four channels for introduction of electrodes. In the lower plate a cavity 6 mm in length, 3 mm in width and 0.1–0.4 mm in depth was dug with a diamond drill. The parts were brought closely into contact with each other by soldering with a gas burner. High purity graphite electrodes (Toyo Tanso, IG430) were employed because of the highly corrosive nature of the liquid As–Te mixtures. The temperature was measured by a chromel–alumel thermocouple, which was in close contact with the cell.

The Hall coefficients were measured by a double ac method, that is, an alternating current and an ac magnetic field. It is advantageous that the Hall voltage is directly detected and

anomalous voltages in the liquids are excluded. The measurement system was composed of three function generators (Hewlett Packard 33120A), a Helmholtz type magnet and a lock-in amplifier (EG&G 7260). The frequency of the current (f_I), frequency of the magnet (f_B) and frequency of the Hall voltage for the lock-in amplifier ($f_H = f_I + f_B$) are adjusted by the function generator. Since the mutual stability of the three frequencies is very important in this system, the three function generators were phase locked to each other. The rms Hall voltage V_H at f_H is given by $V_H = R_H I B/d\sqrt{2}$, where I and B are the rms magnitude of the current to the sample and of the magnetic field, respectively, d is the sample thickness and R_H is the magnitude of the Hall coefficient. The frequency of the current, the magnetic field and the reference signal of the lock-in amplifier were 980, 1 and 981 Hz, respectively. The sensitivity limit is a few nanovolts.

3. Results

3.1. EXAFS for g- and l-$As_{40}Te_{60}$

In figures 1(a) and (b) the As and Te K-edge EXAFS oscillations $k\chi(k)$ for the stoichiometric $As_{40}Te_{60}$ composition at 350 °C, 400 °C, 450 °C and 500 °C are shown as a function of the photoelectron wave number k. The As K-edge EXAFS oscillations are in good agreement with the previous results [12]. The signal-to-noise ratio of the EXAFS spectrum near the Te K edge is comparable to that near the As K edge, while the x-ray intensity corresponding to the energy near the Te K edge (31.8 keV) available at PF in KEK is relatively weak compared with that near the As K edge. Nevertheless, distinct EXAFS oscillation is observed from 3.6 to 12.0 $Å^{-1}$. The oscillations for both K edges are substantially damped with increasing temperature.

Figures 2(a) and (b) show the magnitude of the Fourier transform (FT) of $\chi(k)$, $|F(r)|$, obtained around the central As and Te atoms for l-$As_{40}Te_{60}$ at 350 °C, 400 °C, 450 °C and 500 °C. The $|F(r)|$ curves in figures 2(a) and (b) are asymmetric, in contrast to those of $As_{40}Se_{60}$ shown in figures 3(a) and (b) [25]. As seen in figures 3(a) and (b), both $|F(r)|$ obtained around the central As and Se atoms for l-$As_{40}Se_{60}$ at different temperatures for which the sample was in the supercooled and glassy state has a symmetric peak around 2.5 Å, and the amplitude of the peak decreases with increasing temperature. The one shell curve fitting analysis is enough to derive the structural parameters. The As–Se bond length is deduced to be 2.41 ± 0.01 Å and is independent of temperature, which is in good agreement with previous results [4]. The asymmetric $|F(r)|$ curves for l-$As_{40}Te_{60}$ shown in figures 2(a) and (b) may be caused by the presence of a significant fraction of homopolar Te–Te and As–As bonds. This is supported by the results of $|F(r)|$ for As–Te mixtures with different As concentration which are shown in figures 4(a) and (b). In the case of the As K edge shown in figure 4(a), we note that a shoulder appears for the Te-rich mixtures on the lower distance side of the pseudo-RDFs, suggesting that the existence of As scatterers in the first shell tends to smear out the shoulder with increasing As concentration. In the $|F(r)|$ curve for the Te K edge in the mixture containing 20 at.% As shown in figure 4(b) the peak is split into two parts due to the contribution from Te–As and Te–Te pairs.

These findings are quantitatively supported by the attempt to fit the EXAFS data. Assuming the existence of As–As and As–Te bonds for the As K edge and of Te–As and Te–Te bonds for the Te K edge, the two shell curve fitting analysis has been carried out in the k-range from 3.6 to 12.6 $Å^{-1}$ using the theoretical parameter calculated by the FEFF6 code [24]. In figure 5 the theoretical fitting curve denoted by a full line is compared with experimental points $k\chi(k)$ for the Te K edge of l-$As_{40}Te_{60}$ at 450 °C. As seen in the figure the agreement is satisfactory. The As–Te, As–As and Te–Te bond lengths at the stoichiometric $As_{40}Te_{60}$

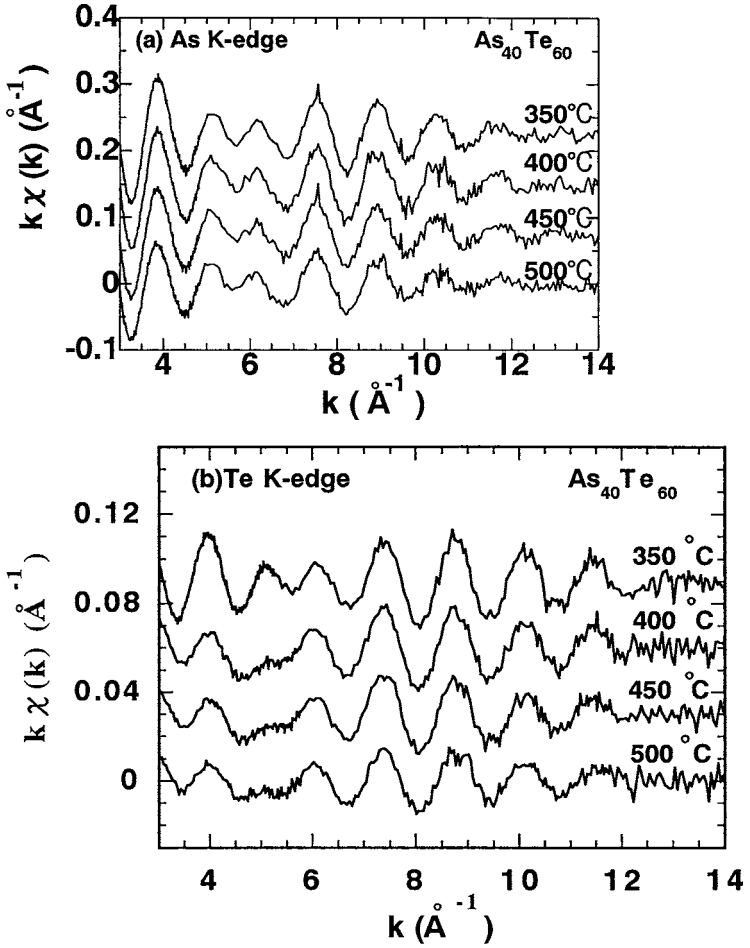

Figure 1. The EXAFS oscillations $k\chi(k)$ around the central (a) As atom and (b) Te atom for l-$As_{40}Te_{60}$ at different temperatures.

composition are estimated to be 2.63, 2.47 and 2.74 ± 0.01 Å and are nearly independent of temperature. Our results for g-$As_{40}Te_{60}$ are in fairly good agreement with data by Ma *et al* [9]. Figure 6(a) shows the temperature variation of the coordination number $N_{As(tot)=(As-Te)+(As-As)}$ for the sum of Te and As around the central As atoms, and the partial coordination number N_{As-Te} for Te and N_{As-As} for As around the central As atoms for l-$As_{40}Te_{60}$ including temperatures where the samples were in supercooled and glassy states. It is noticed that N_{As-As} is equal to ∼1 and is nearly independent of temperature in the liquid state as well as in the glassy state, which implies that stable homopolar As–As pairs exist in the first coordination shell in the g- and l-$As_{40}Te_{60}$. Below the glass transition temperature T_g, $N_{As(tot)}$ around As atoms is about 3. It drops to 2.6 near the melting point T_m (381 °C) and decreases to 2.0 around 500 °C. Figure 6(b) shows the coordination number $N_{Te(tot)=(Te-As)+(Te-Te)}$ for the sum of As and Te around the central Te atoms and the partial coordination number N_{Te-As} for As, N_{Te-Te} for Te around the central Te atoms in the wide temperature range from liquid nitrogen temperature to 500 °C. The Te coordination number $N_{Te(tot)}$ around the central Te atoms for g-$As_{40}Te_{60}$ is 2. Above T_g, $N_{Te(tot)}$ rapidly decreases from 2 and to ∼1 around 500 °C. In the

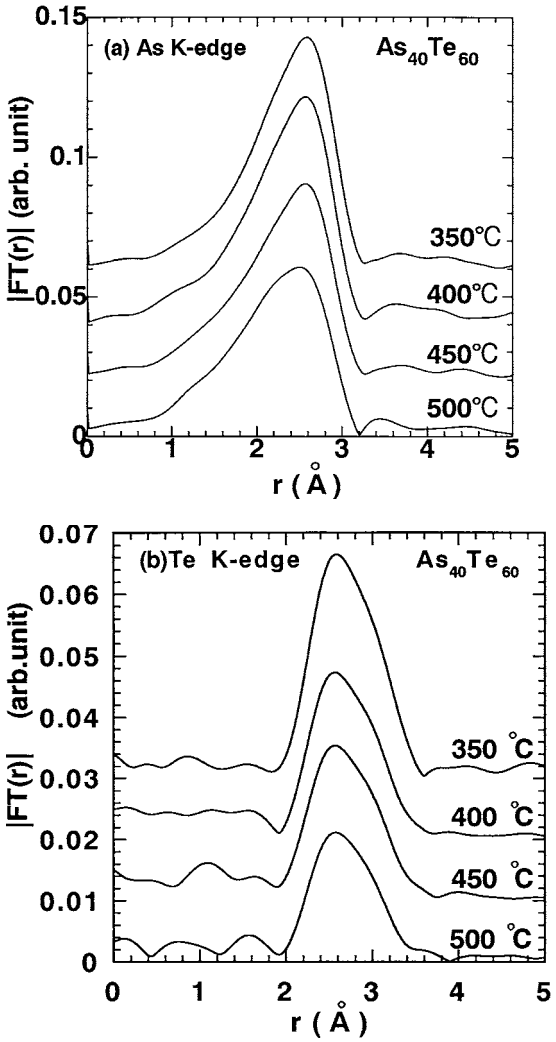

Figure 2. The magnitude of the Fourier transforms of EXAFS around the central (a) As atom and (b) Te atom for l-$As_{40}Te_{60}$ at different temperatures.

glassy state the As coordination number marked by the simultaneous existence of As–As and As–Te pairs is 3 and the Te coordination number marked by the simultaneous existence of Te–Te and Te–As pairs is 2. In the liquid state, however, the network structure in g-$As_{40}Te_{60}$ composed of threefold coordinated As atoms and twofold coordinated Te atoms is transformed into the twofold chain structure at high temperature. Figure 7 shows the temperature variation of mean square displacement σ^2 for neighbouring atoms around Te atoms for l-$As_{40}Te_{60}$. As seen in figure 7 σ^2 for Te–Te pairs increases rapidly above 450 °C, which is related to the fact that the Te–Te bond is weak compared to the As–Te bond and disrupts easily at high temperature. Structural parameters such as coordination number N, bond length r and root mean square displacement σ for g- and l-$As_{40}Te_{60}$ are compiled in table 1.

Important findings obtained from EXAFS analysis for g- and l-$As_{40}Te_{60}$ are as follows: (a) a significant level of chemical disorder, marked by the existence of homopolar As–As and

Table 1. Structural parameters (N: coordination number, r: bond length, σ: root mean square displacement) for g- and l-$As_{40}Te_{60}$.

		As–As			As–Te			Te–As			Te–Te		
	T (°C)	N	r (Å)	σ (Å)	N	r (Å)	σ (Å)	N	r (Å)	σ (Å)	N	r (Å)	σ (Å)
g-$As_{40}Te_{60}$	25	1.15	2.47	0.035	1.84	2.63	0.047	1.23	2.63	0.049	0.69	2.75	0.058
	75	1.08	2.47	0.035	1.76	2.64	0.051	1.29	2.64	0.051	0.67	2.74	0.068
	100	1.13	2.48	0.050	1.76	2.63	0.052	1.22	2.63	0.055	0.70	2.75	0.076
l-$As_{40}Te_{60}$	400	1.08	2.48	0.066	1.40	2.62	0.081	0.99	2.62	0.076	0.45	2.72	0.086
	450	1.05	2.48	0.068	1.36	2.62	0.085	0.94	2.62	0.077	0.55	2.73	0.088
	500	0.96	2.47	0.068	1.06	2.63	0.088	0.80	2.62	0.080	0.37	2.72	0.103
	550	0.88	2.46	0.074	0.96	2.64	0.095						

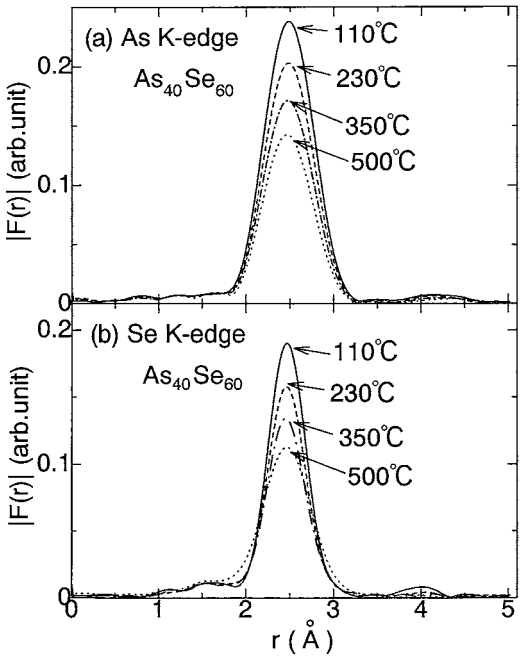

Figure 3. The magnitude of the Fourier transforms of EXAFS around the central (a) As atom and (b) Se atom for l-$As_{40}Se_{60}$ at different temperatures.

Te–Te pairs in the first coordination shell, is observed; (b) in the liquid state around 500 °C, the network structure is transformed into the chain structure composed of twofold coordinated As atoms and onefold coordinated Te atoms ('network–chain' transformation). Of particular interest this structural transition is accompanied by the S–M transition which is demonstrated by the results for conductivity and Hall coefficient as described later. The bonding configuration of Te atoms is considered to primarily govern the S–M transition. The width of the band gap is determined, to a large extent, by the strength of the bonds. The increase of the number of weak Te–Te bonds may cause shrinkage of the band gap. Therefore a detailed knowledge of the local environment around Te and As atoms in the liquid mixture with different As concentration allows a helpful understanding of the involved mechanism of the S–M transition.

3.2. EXAFS for l-As_xTe_{100-x} mixtures

Figure 8(a) shows the temperature variation of the coordination number around the central As atom for l-$As_{20}Te_{80}$. The partial coordination number $N_{\mathrm{As–As}}$ is nearly independent of temperature, which suggests that stable homopolar As–As pairs exist in the first coordination shell. The partial coordination number $N_{\mathrm{As–Te}}$ decreases with increasing temperature. As a result, $N_{\mathrm{As(tot)}}$ around the central As atoms reduces from 2.6 to 380 °C to 2.0 around 500 °C. We suggest that l-$As_{20}Te_{80}$ undergoes 'network–chain' transformation around 500 °C. As shown in figure 8(b) the partial coordination numbers $N_{\mathrm{Te–Te}}$ and $N_{\mathrm{Te–As}}$ decrease with increasing temperature and $N_{\mathrm{Te(tot)}}$ reduces to 1 around 500 °C. Since the Te–Te bonds are significantly weak compared to the As–As and As–Te ones, a large fraction of Te–Te bonds in the chain is broken by thermal agitation at high temperature. The value of $N_{\mathrm{Te–Te}}$ for l-$As_{20}Te_{80}$, which is very rich in Te content, is 0.6 around 500 °C as seen in figure 8(b). This is extremely

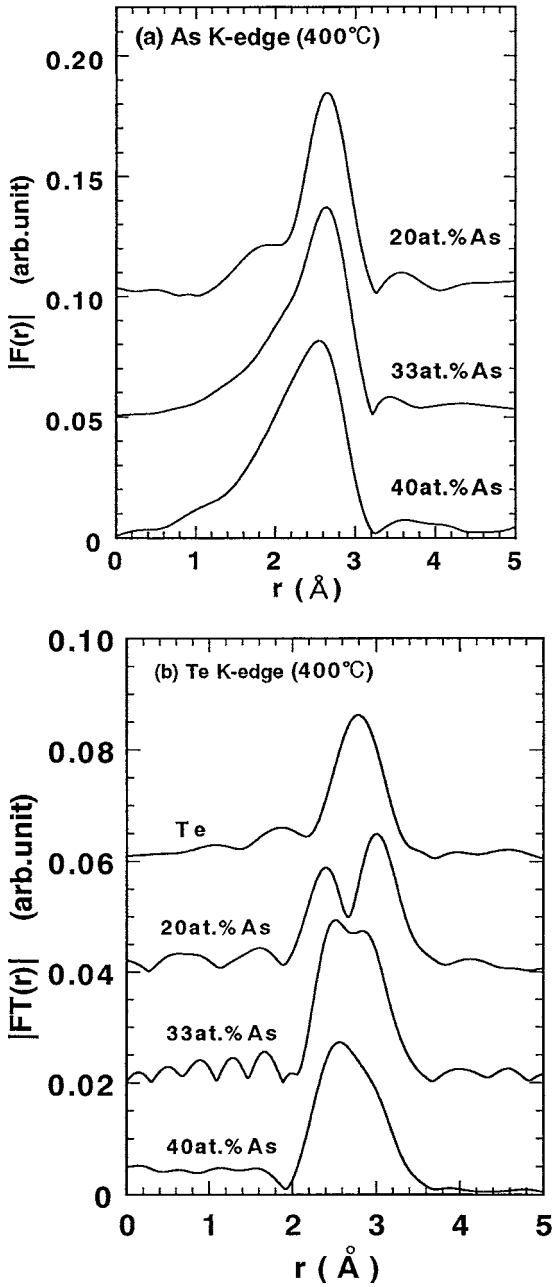

Figure 4. The magnitude of the Fourier transforms of EXAFS around the central (a) As atom and (b) Te atom for l-As_xTe_{100-x} mixtures at 400 °C at different concentrations.

small. The EXAFS experiments on pure liquid Te [18] show that the chains in liquid Te with metallic properties are composed of short and long covalent bonds and the total coordination number (sum of the coordination numbers for short and long bonds) is 1.8 at 500 °C. A large fraction of the long bond in l-Te is considered to be broken upon the addition of As to liquid Te.

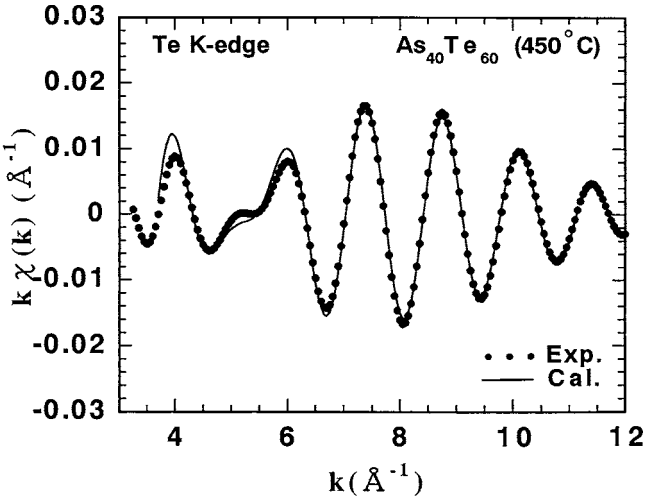

Figure 5. Fourier filtered K-edge EXAFS oscillation $k\chi(k)$ for l-$As_{40}Te_{60}$ at 450 °C and the fitting curve. The full line denotes the results of the curve fit and solid circles denote experimental points.

Figures 9(a) and (b) show the coordination numbers around the central As atoms and Te atoms for l-$As_{33}Te_{67}$ in the temperature range between 400 and 600 °C. The results also provide the possibility that the 'network–chain' transformation occurs at 500–550 °C.

Figure 10(a) shows the compositional dependence of $N_{\mathrm{As–Te}}$, $N_{\mathrm{As–As}}$ and $N_{\mathrm{As(tot)}}$ for l-As_xTe_{100-x} mixtures at 500 °C. When one extrapolates the curves for $N_{\mathrm{As–Te}}$ and $N_{\mathrm{As–As}}$ to 50 at.% As content, both $N_{\mathrm{As–Te}}$ and $N_{\mathrm{As–As}}$ approach 1 keeping $N_{\mathrm{As(tot)}} \sim 2$ in the concentration range up to 50 at.% As. In figure 10(b) $N_{\mathrm{Te(tot)}}$, $N_{\mathrm{Te–As}}$ and $N_{\mathrm{Te–Te}}$ at 500 °C are shown as a function of As concentration. Of particular interest $N_{\mathrm{Te–As}}$ tends to 1 and $N_{\mathrm{Te–Te}}$ decreases with increasing As content. For concentration more than 50 at.% As, however, the Te–Te bonds still exist probably until 66 at.% As corresponding to As_2Te as found by a linear extrapolation of the $N_{\mathrm{Te–Te}}$ curve.

3.3. Temperature and pressure variation of dc conductivity σ_{dc}

Figure 11 shows a plot of log σ_{dc} against the reciprocal temperature $1/T$ for l-Te, l-$As_{10}Te_{90}$, l-$As_{20}Te_{80}$, l-$As_{33}Te_{67}$ and l-$As_{40}Te_{60}$. Our results are in good agreement with those of Oberafo [26]. The values of σ_{dc} for l-As_xTe_{100-x} mixtures are small at low temperature and reduce substantially with increasing As concentration. With increasing temperature, σ_{dc} of l-As_xTe_{100-x} mixtures rapidly increases and reaches $\sim 10^3\ \Omega^{-1}\ \mathrm{cm}^{-1}$ at high temperature. The curves for log σ_{dc}–$1/T$ deviate from a linear function at high temperature, suggesting transition from the semiconducting to metallic state. The temperature where σ_{dc} curves begin to deviate from a straight line moves to higher temperature with As concentration, that is, the S–M transition occurs at higher temperature for the mixtures containing higher As concentration. Figures 12 and 13 show the pressure variation of σ_{dc} for $As_{20}Te_{80}$ and $As_{40}Te_{60}$ at different temperatures. Above 500 °C σ_{dc} increase with increasing pressure for l-$As_{20}Te_{80}$ and l-$As_{40}Te_{60}$, though σ_{dc} decreases slightly at comparatively low temperature below 500 °C on application of pressure.

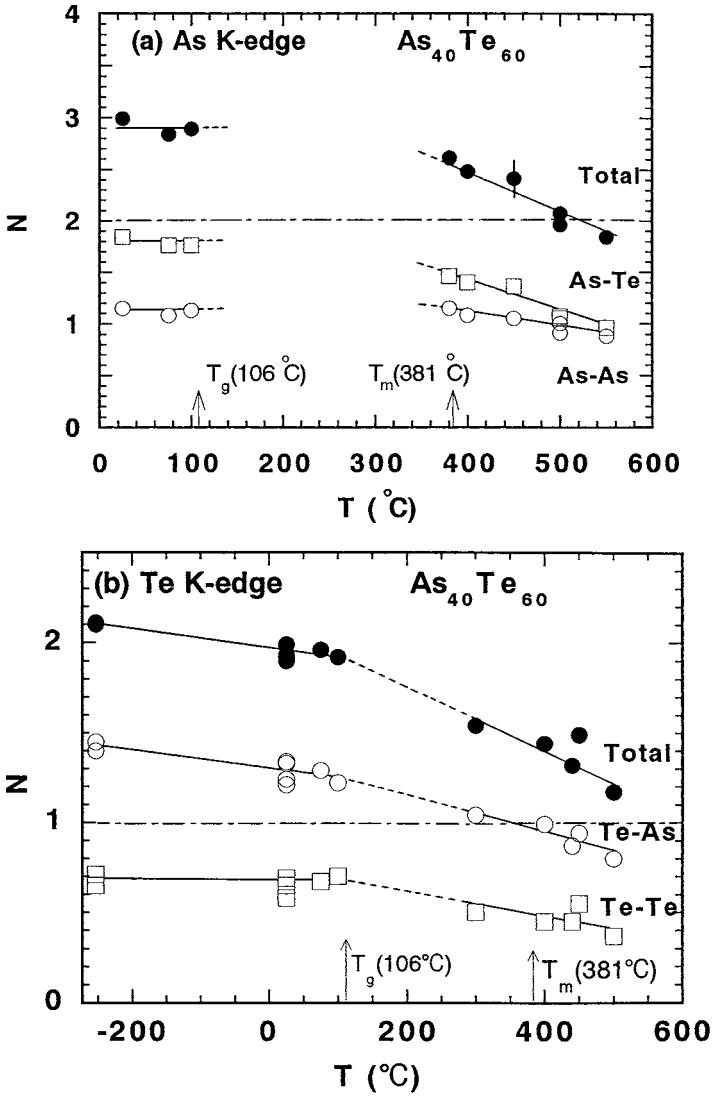

Figure 6. Temperature variations of the coordination number N around (a) the As atom and (b) the Te atom for l-$As_{40}Te_{60}$. Solid circles indicate N_{tot}, open circles indicate $N_{As–As}$ in (a) and $N_{Te–As}$ in (b), open squares indicate $N_{As–Te}$ in (a) and $N_{Te–Te}$ in (b). Full, broken and chain lines are drawn as guides for the eye.

3.4. Hall coefficient and S–M transition

The measurement of Hall coefficient (R_H) is a complement to the measurement of σ_{dc} and is a good means of understanding the microscopic transport, since it depends on the conduction affected by the topological geometry of atoms according to Friedman [27]. Figure 14 shows the temperature dependence of $|R_H|$ for l-As_xTe_{100-x} with various concentrations of As. The sigh of R_H for l-As_xTe_{100-x} mixtures is negative despite the p-type thermoelectric power [26]. The value of $|R_H|$ increases with increasing As concentration. As seen in the figure, there are three regimes, I, II and III, in the temperature dependence. Regime I has a smaller temperature

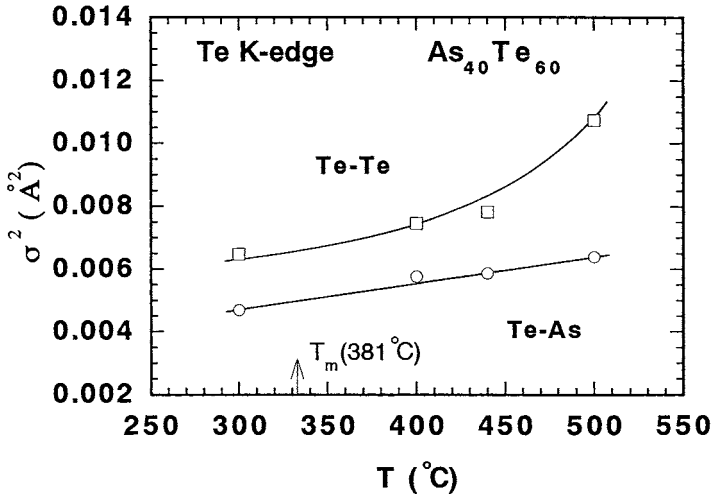

Figure 7. Temperature variations of the mean square displacement σ^2 around the Te atom for l-$As_{40}Te_{60}$. Open circles indicate $N_{Te–As}$ and open squares indicate $N_{Te–Te}$. Full lines are drawn as guides for the eye.

dependence than the other two. In regime II a rapid decrease of $|R_H|$ is seen. The boundary denoted by the arrow in the figure between regime I and II may correspond to the onset of the S–M transition. The transition temperatures which are indicated by arrows lie around 350 °C for l-Te, 380 °C for l-$As_{10}Te_{90}$, 410 °C for l-$As_{20}Te_{80}$ and 450 °C for l-$As_{30}Te_{70}$, which are close to the 'network–chain' transformation temperature. This encourages us to believe that the S–M transition is accompanied by the 'network–chain' transformation. The Hall mobility μ_H can be deduced from the equation $\mu_H = |R_H|\sigma_{dc}$. Figure 15 shows a plot of log μ_H against the reciprocal temperature $1/T$ for l-Te, $As_{10}Te_{90}$, $As_{20}Te_{80}$ and $As_{30}Te_{70}$. The value of μ_H for l-Te is 0.2 $cm^2\ V^{-1}\ s^{-1}$ and is nearly independent of temperature. For the liquid mixtures containing As, log μ_H–$1/T$ curves show a linear temperature dependence at lower temperature and have maxima. At high temperature μ_H becomes nearly independent of temperature as for l-Te. The temperature where there appears a maximum in μ_H moves towards higher temperature with increasing As concentration. These results suggest that the conduction mechanism in l-As_xTe_{100-x} mixtures changes at high temperatures.

4. Discussion

The analysis of $|F(r)|$ derived from EXAFS data for $As_{40}Te_{60}$ reveals that the As coordination number is about 3 and the Te coordination number is about 2 in the glassy state. In the liquid state at high temperature (∼500 °C) such a network structure transforms to a chainlike structure by breaking of As–Te bonds, keeping strongly bonded As pairs intact. This is also confirmed for l-As_xTe_{100-x} mixtures with various As concentrations as shown in figures 6, 8 and 9.

There is a significant level of chemical disorder in l-As_xTe_{100-x} mixtures, marked by the existence of homopolar As–As and Te–Te pairs in the first coordination shell. The bonding energies reported in the literature [28] are 47.7 kcal mol^{-1} for As–As, 45 kcal mol^{-1} for As–Te and 38 kcal mol^{-1} for Te–Te bonds. The present EXAFS results demonstrate a clear tendency which is in good agreement with the bonding energy values. As shown in table 1, the root mean square displacement σ for Te–Te pairs in liquid mixtures is large and has a strong

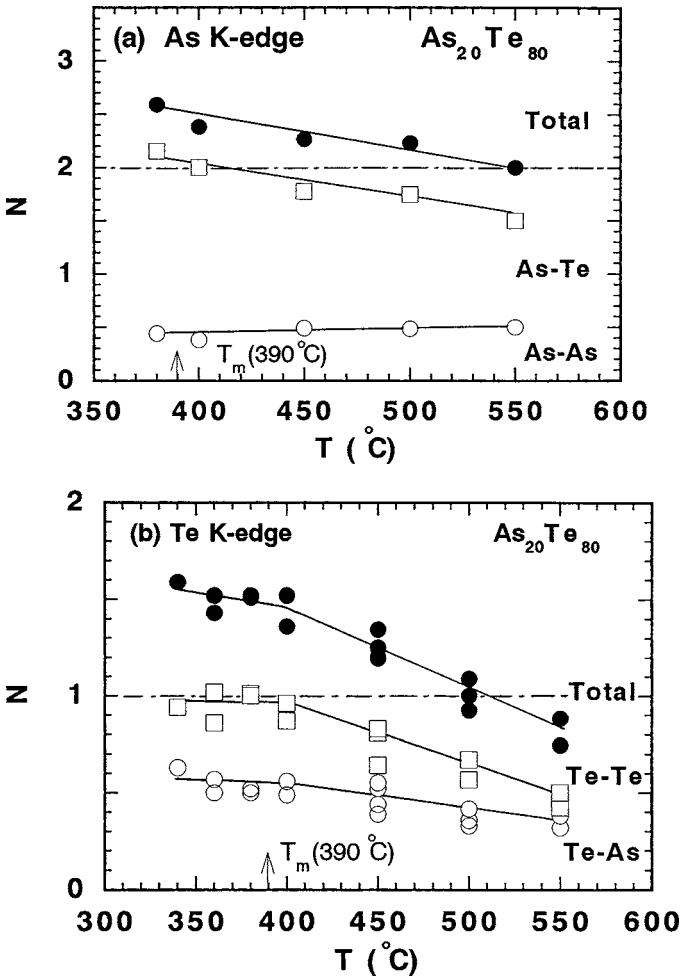

Figure 8. Temperature variations of the coordination number N around (a) the As atom and (b) the Te atom for l-$As_{20}Te_{80}$. Solid circles indicate N_{tot}, open circles indicate $N_{As–As}$ in (a) and $N_{Te–As}$ in (b), open squares indicate $N_{As–Te}$ in (a) and $N_{Te–Te}$ in (b). Full and chain lines are drawn as guides for the eye.

temperature dependence at high temperature compared with those for As–As and As–Te pairs, which indicates that the Te–Te bond is weaker since larger σ is related to larger fluctuations of the bonding distances. The large difference in the bonding energies between As–Te and Te–Te bonds makes As atoms more likely to bind to Te atoms. The partial coordination number around Te, $N_{Te–Te}$, reduces substantially upon the addition of As as seen in figure 10(b) and tends to 0 in As-rich concentration. On the other hand, the coordination numbers around As atoms $N_{As–Te}$ and $N_{As–As}$ approach 1 at 50 at.% As keeping $N_{As(tot)}$ as 2 (see figure 10(a)). These results suggest that there appears in As-rich liquid mixtures a local atomic arrangement such as Te–As–As–Te whose both ends of –As–As– are terminated by Te atoms. Thus it is considered that Te–Te bonds are less favoured while As–As and As–Te are more favoured. Te atoms within a chain are not randomly replaced by As atoms since As–As pairs are more favoured. In contrast to liquid As_xTe_{100-x} mixtures, $|F(r)|$ obtained around the central As and Se atoms for l-$As_{40}Se_{60}$ has a symmetric peak around 2.5 Å. The bonding energies [29] are 52 kcal mol^{-1}

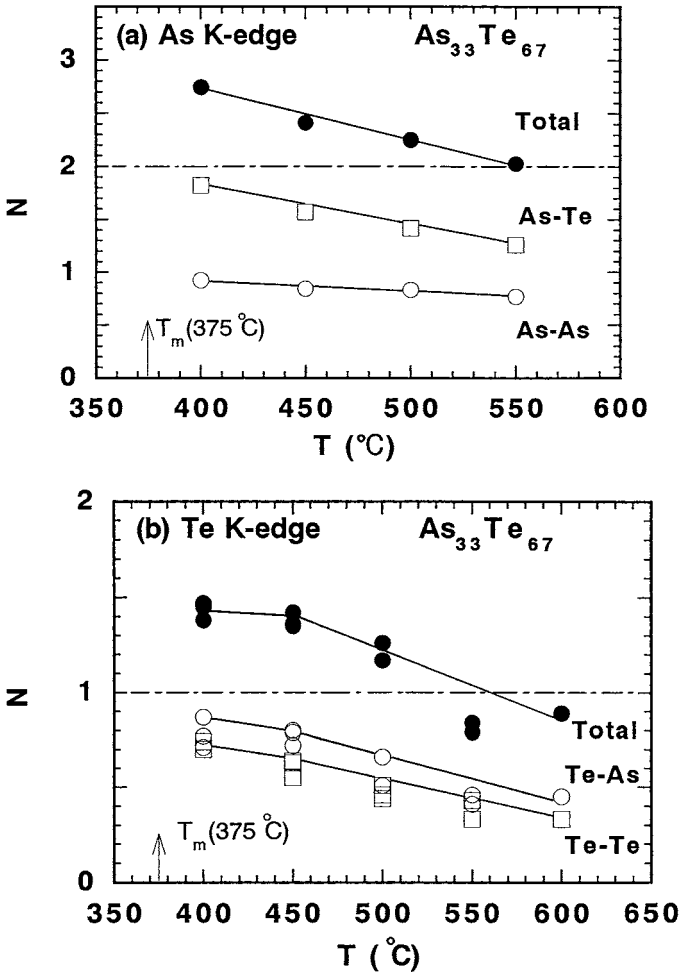

Figure 9. Temperature variations of the coordination number N around (a) the As atom and (b) the Te atom for l-$As_{33}Te_{67}$. Solid circles indicate N_{tot}, open circles indicate $N_{As–As}$ in (a) and $N_{Te–As}$ in (b), open squares indicate $N_{As–Te}$ in (a) and $N_{Te–Te}$ in (b). Full and chain lines are drawn as guides for the eye.

for As–Se, 49 kcal mol^{-1} for Se–Se and 46 kcal mol^{-1} for the As–As bond. The differences in these energies show that As–Se bonds are more favoured resulting in chemical order.

Recently, Tsuchiya [30, 31] has carried out the measurements for the densities and sound velocities of l-As_xTe_{100-x} mixtures and found that the volume contracts and the adiabatic compressibility κ_S derived from the sound velocity shows a maximum near the S–M transition temperature in the same manner as observed for l-Se_xTe_{100-x} mixtures [32, 33]. In figure 16 the boundary where the gradual S–M transition occurs in l-As_xTe_{100-x} mixtures is shown by a hatched region on the temperature–concentration plane. The S–M transition temperatures determined from the $|R_H|$–T curves which are denoted by arrows in figure 14 are in good agreement with those from κ_S–T curves [31]. The transition temperatures move to higher temperature with increasing As concentration. As seen in figure 15 μ_H for l-As_xTe_{100-x} have maxima in the vicinity of S–M transition temperatures. Although all regimes (I, II and III) are not covered over an entire concentration range of As as seen in figure 14, the most convincing

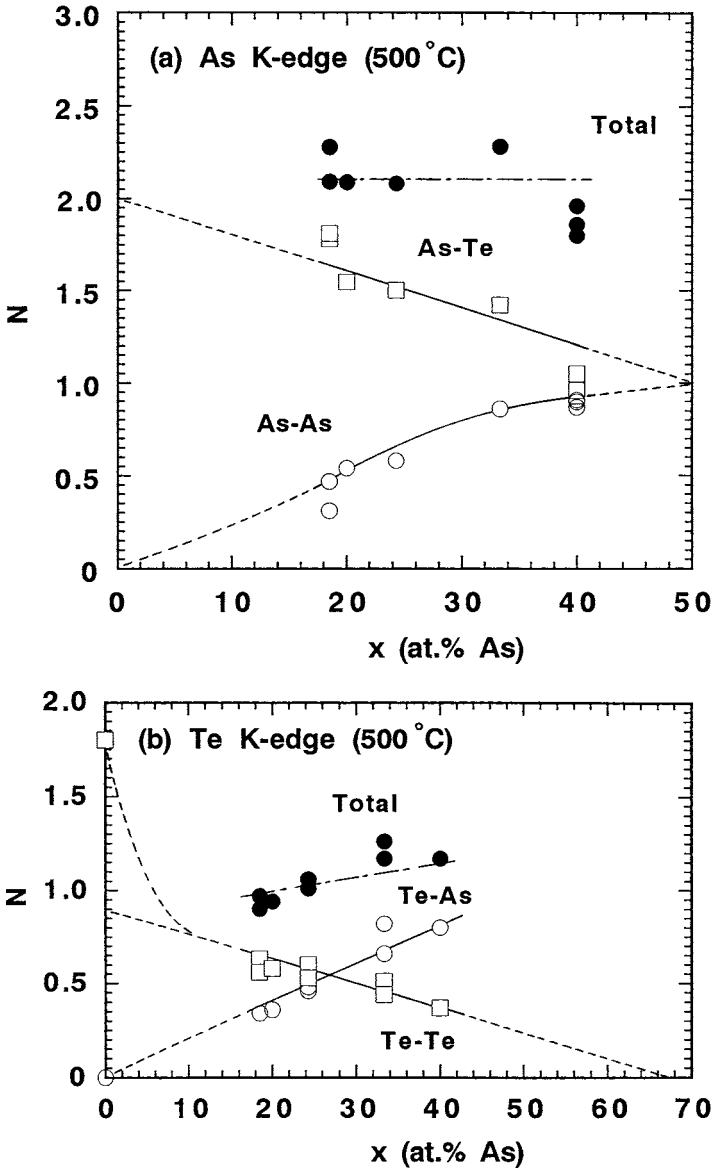

Figure 10. Concentration variations of the coordination number N around (a) the As atom and (b) the Te atom for l-As_xTe_{100-x} mixtures at 500 °C. Solid circles indicate N_{tot}, open circles indicate N_{As-As} in (a) and N_{Te-As} in (b), open squares indicate N_{As-Te} in (a) and N_{Te-Te} in (b). Full, broken and chain lines are drawn as guides for the eye.

evidence for the S–M transition can be obtained from $|R_H(\sigma_{dc})|$ curves as shown in figure 17. The $|R_H|$ data for all mixtures bend downward around 350 Ω^{-1} cm^{-1}, corresponding to the so-called minimum metallic conductivity, and decrease to a much smaller value. When $|R_H|$ data are extrapolated by a linear function, they converge on $R_H = -5 \times 10^{-11}$ m^3 C^{-1} and $\sigma_{dc} = 5000$ Ω^{-1} cm^{-1}.

The sign of the Hall coefficient of the liquid mixtures is negative, i.e. opposite in sign to the observed thermopower [26]. The random phase model has been proposed by Friedman [27] to

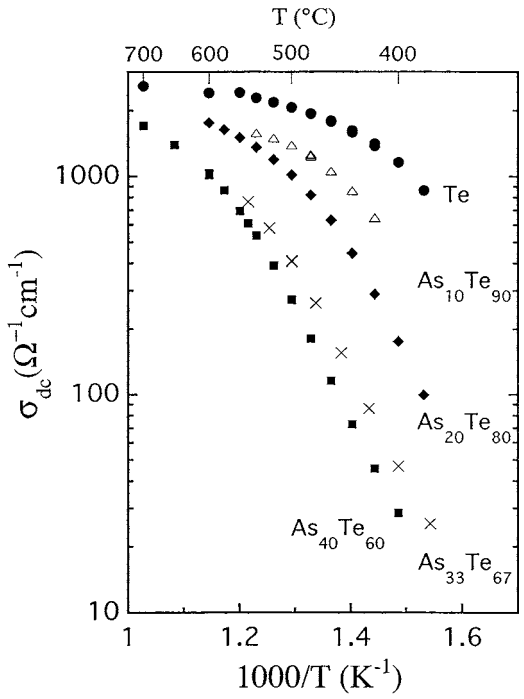

Figure 11. Temperature variations of the dc conductivity σ_{dc} for l-As_xTe_{100-x} mixtures as a function of reciprocal absolute temperature.

explain the sign of Hall coefficient and the temperature variation of the Hall mobility in liquid semiconductors and semimetals. The model is given by

$$\mu_H \simeq 2\pi \left(\frac{ea^2}{\hbar}\right)\left(\frac{W}{V_0}\right)\left(\frac{\eta\tilde{z}}{z^2}\right) \simeq \text{constant}\left(\frac{ea^2}{\hbar}\right) \tag{6}$$

where a is the average interatomic spacing, W is equal to $2zJ$ where J is the transfer integral between sites, V_0 is a measure of the disorder potential, η is a parameter <1, $\tilde{z}$ is the average number of sites forming a closed path and z is the nearest-neighbour coordination number. For three-site configurations R_H is always negative, whether the moving particles are electrons or holes. If it is assumed that values of (W/V_0), η, $\tilde{z}$ and z are not expected to vary significantly, one can write $(W/V_0)(\eta\tilde{z}/z^2)$ as a constant. Note that for this mechanism μ_H has no dependence on temperature. In fact, μ_H for liquid metallic Te is independent of temperature as seen in figure 15. The log μ_H–$1/T$ curves for l-As_xTe_{100-x} mixtures show linear temperature dependence at low temperature, which suggests that most of the current is carried by hole hopping at the band edge at low temperature [1]. It should be noted that μ_H for liquid mixtures decreases with increasing temperature and tends to be nearly independent of temperature as for l-Te at high temperature.

The metallic properties of l-Te arise from the strong interactions among the chains shortened by thermal agitation. When temperature is lowered from the melting point to the supercooled state, l-Te undergoes a transition from metal to semiconductor, accompanied by a volume change. The EXAFS analysis [18] suggests that the short chains in l-Te with metallic nature are composed of the same number of short (∼2.80 Å) and long (∼2.95 Å) covalent bonds and that the long bonds vanish in the semiconducting state at low temperature. In Te and Se, two of the four p electrons form the σ-bonds between neighbouring atoms and the

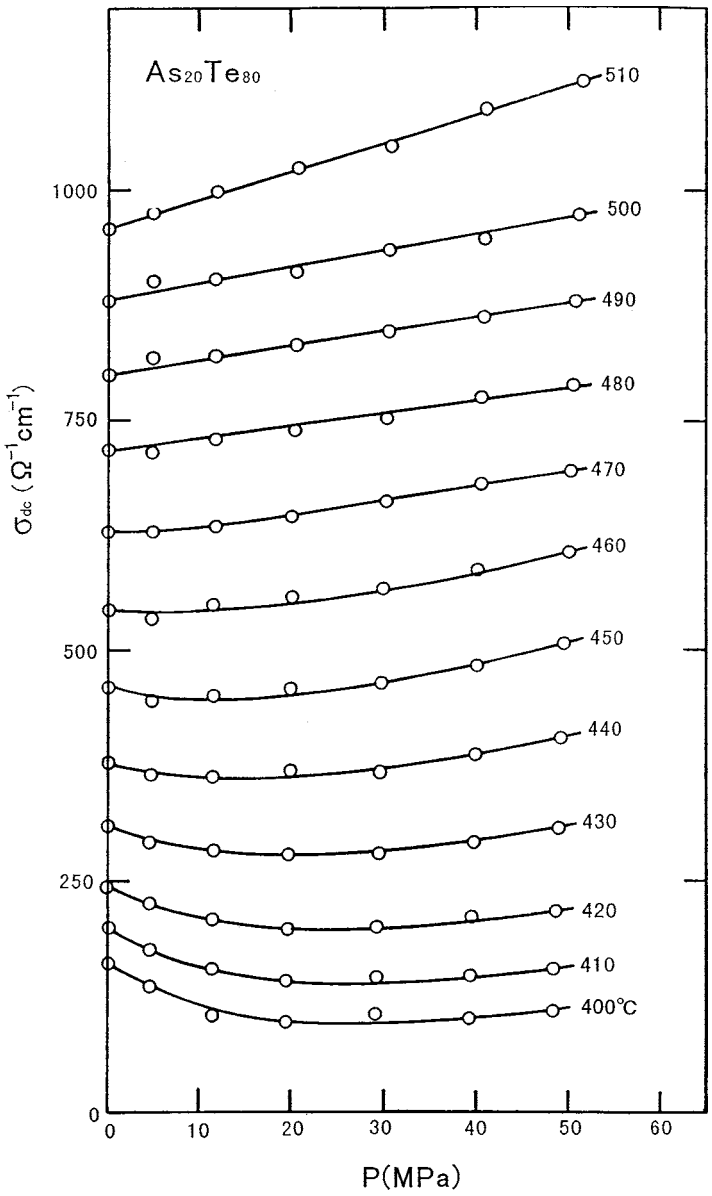

Figure 12. Pressure variations of the dc conductivity σ_{dc} for l-$As_{20}Te_{80}$ at different temperatures. Full lines are drawn as guides for the eye.

retained two electrons occupy the lone pair (LP) orbital. In liquid metallic Te, a frequent charge transfer from LP orbitals to antibonding orbitals in the neighbouring chains occurs by thermal agitation. The chains are composed of only a few atoms at high temperature. The average chain length of l-Te is estimated to be about ten atoms by Misawa [34] and three atoms by Cutler *et al* [35] just above the melting point. The chain ends carry negative charge and the mid-chain atoms have a corresponding positive charge associated with a hole, since an electron tends to be transferred into the p orbital of the broken bonds. The inter- and intra-charge transfers result in fluctuations of charge distribution in the chain molecule: creation of

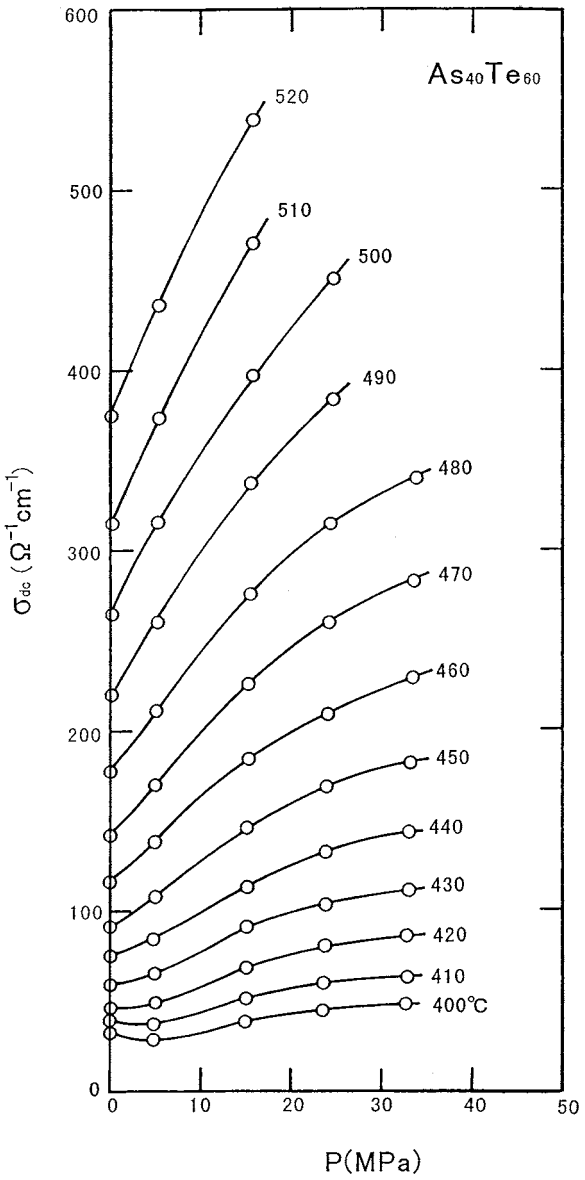

Figure 13. Pressure variations of the dc conductivity σ_{dc} for l-$As_{40}Te_{60}$ at different temperatures. Full lines are drawn as guides for the eye.

long bonds (three-electron σ-bonds [36]) and holes in the LP orbitals. As a result, volume contraction is induced by the attractive force between the polarizable chains.

We give a possible explanation for the source of the S–M transition in l-As_xTe_{100-x} mixtures along the same lines as discussed above for that in liquid Te. A substantial decrease of N_{Te-Te} is observed upon the addition of As as shown in figure 10(b). When the N_{Te-Te} curve in figure 10(b) is extrapolated linearly to $x = 0$ as denoted by the dotted line, we find $\sim$0.9 for N_{Te-Te}, which is half of the total coordination number ($\sim$1.8) of pure l-Te. This implies that long bonds substantially reduce upon the addition of As owing to the significant difference

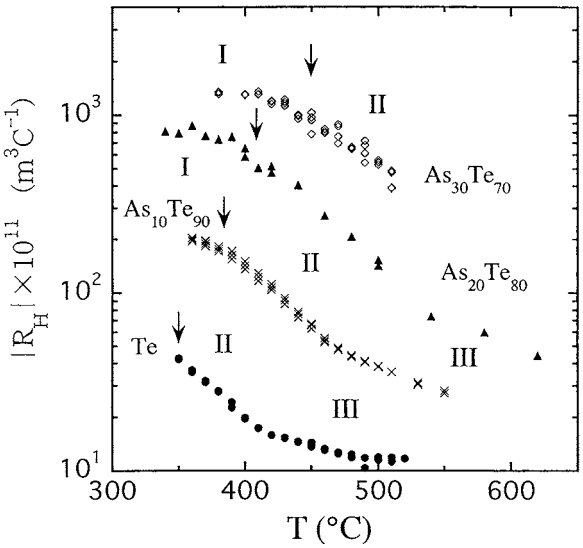

Figure 14. Temperature variations of Hall coefficient $|R_H|$ of l-As_xTe_{100-x} mixtures. The arrows indicate the onset of the semiconductor–metal transition. The symbols I, II and III denote the regions discussed in the text.

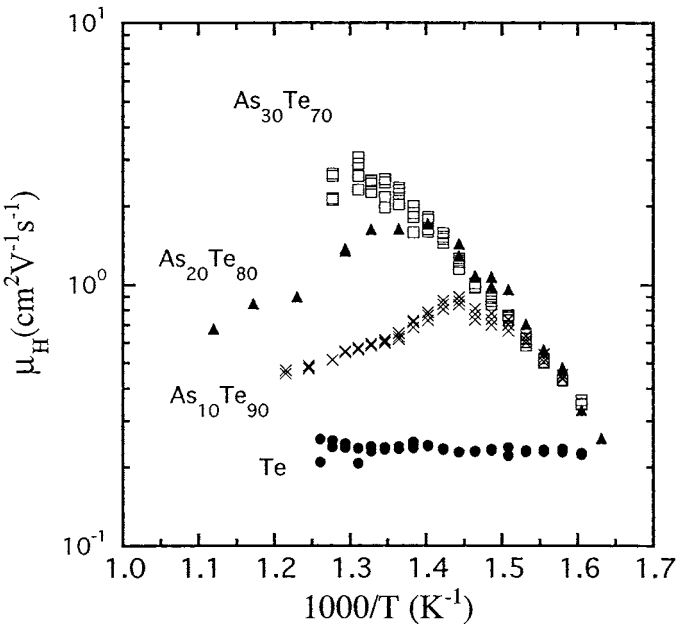

Figure 15. Temperature variations of Hall mobility μ_H of l-As_xTe_{100-x} mixtures.

in the bonding energies between As–Te and Te–Te bonds. The electrons around Te atoms tend to be promoted to half-filled p-like non-bonding states around the twofold coordinated As atoms produced by the 'network–chain' transformation, while Te atoms at the chain ends tend to carry negative charge. The fluctuations of charge distribution result in strong inter-chain coupling. Therefore, the volume contracts and hole conduction through LP bands is

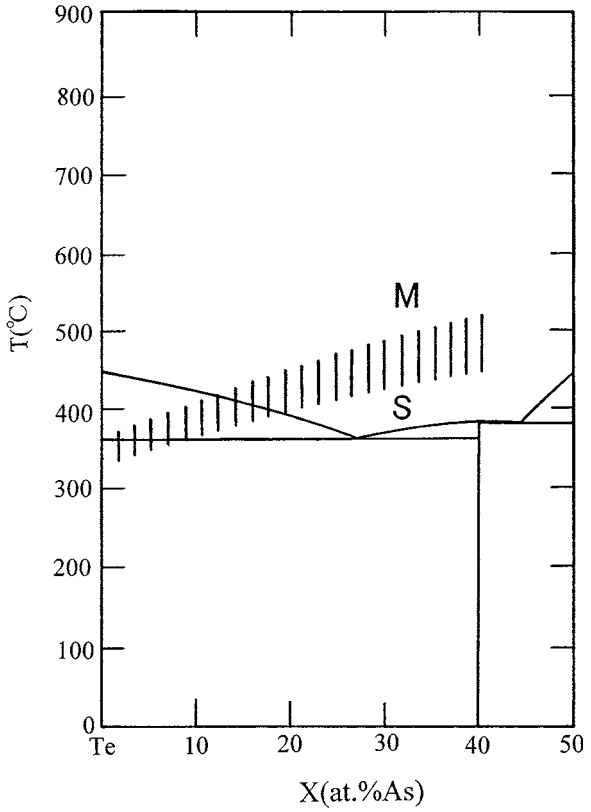

Figure 16. The region of the semiconductor (S)–metal (M) transition on the phase diagram of l-As_xTe_{100-x} mixture.

induced. This is our scenario for the source of the S–M transition in the liquid As–Te mixtures composed of covalently bonded chains. The metallic conductivity observed for l-As_xTe_{100-x} mixtures may be mainly determined by the conduction path along the inter-chain direction, which is confirmed by the measurements for σ_{dc} under pressure as shown in figures 12 and 13. The σ_{dc}–P curves for l-$As_{20}Te_{80}$ and l-$As_{40}Te_{60}$ show that σ_{dc} increases on applying pressure, though it decreases initially. The increase of σ_{dc} on compression is related to the increase of the overlaps of LP orbitals and the substantial increase of the number of charge carriers (holes) which bear the metallic character in the sense of the transport property.

5. Conclusion

The studies have been focused on the links between the structural aspects of l-As_xTe_{100-x} mixtures and their electronic properties. EXAFS data demonstrate the presence of chemical disorder marked by the existence of homopolar As–As and Te–Te pairs in l-As_xTe_{100-x} mixtures. In the liquid state at high temperature the network structure composed of threefold coordinated As atoms and twofold coordinated Te atoms is transformed into the twofold chain structure. The temperature where the 'network–chain' transformation occurs moves to higher temperature with increasing As concentration. The chains are very short at high temperature and the chain ends are terminated by Te atoms in As-rich mixtures. These results can be

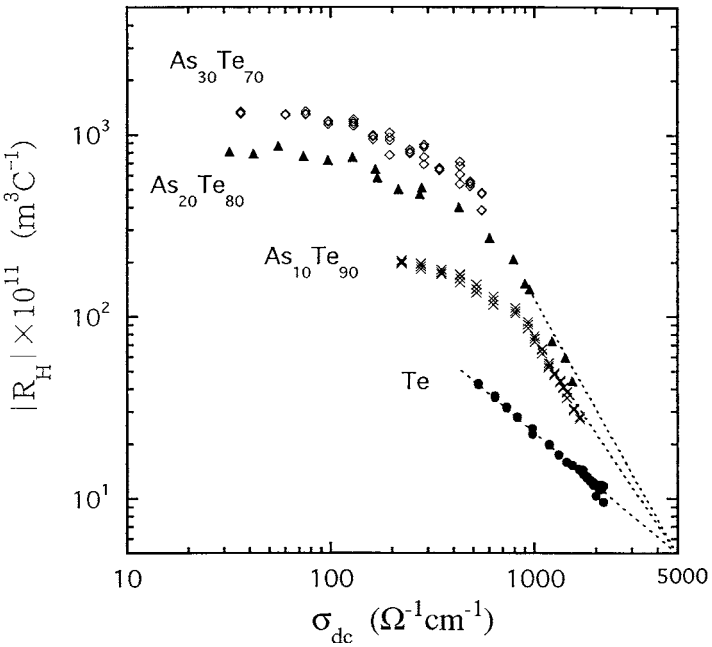

Figure 17. Plots of $|R_{\mathrm{H}}|$ versus σ_{dc} for l-As_xTe_{100-x} mixtures. Broken lines are drawn as guides for the eye.

understood by taking into account the significant difference in bonding energies among As–As, As–Te and Te–Te bonds. The 'network–chain' transformation is associated with the S–M transition which is proved by the conductivity and Hall coefficient measurements. The $\log \sigma_{\mathrm{dc}}$ versus $1/T$ curves for l-As_xTe_{100-x} mixtures deviate from the linear function at high temperature. Furthermore the measurements for σ_{dc} under pressure reveal that σ_{dc} increases on compression. The Hall mobility μ_{H} deduced from R_{H} data for l-Te with metallic nature is independent of temperature. The curves of $\log \mu_{\mathrm{H}}$ versus $1/T$ for the liquid mixtures containing As lie on a straight line at low temperature. At high temperature, μ_{H} for l-As_xTe_{100-x} mixtures have maxima and tend to be independent of temperature as for metallic l-Te on further raising temperature, suggesting a change of the conduction mechanism. The maximum of μ_{H} moves to higher temperature with increasing As concentration.

Based on our results we suggest a possible explanation for the source of the S–M transition observed for l-As_xTe_{100-x} mixtures. The half-filled p-like non-bonding states around twofold coordinated As atoms are modified by 'network–chain' transformation and the dangling bonds of Te cause large fluctuations of the charge distribution in the shortened chains, which results in a frequent inter- and intra-charge transfer. We conclude that the S–M transition is induced by a substantial increase of the number of charge carriers and the metallic conduction path is mainly along the inter-chain direction.

Acknowledgments

This work was supported by a Grant-in-Aid for Scientific Research (C) from the Ministry of Education, Science, Sports, and Culture of Japan. One of the authors (HH) is indebted to Nippon Sheet Glass Foundation for Materials Science and Engineering for partial financial support. This work was performed under the approval of proposal Nos 94G208, 96G164

and 98G294 of the Photon Factory (PF) at KEK. The authors wish to thank Mr S Yamamoto (Nippon Engineering) for his technical assistance with the Hall coefficient measurements.

References

[1] Mott N F and Davis E A 1979 *Electronic Processes in Non-Crystalline Materials* (Oxford : Clarendon)
[2] Ikemoto H, Hoshino H, Miyanaga T, Yamamoto I and Endo H 1999 *J. Non-Cryst. Solids* **250–252** 458
[3] Hosokawa S, Sakaguchi Y and Tamura K 1992 *J. Non-Cryst. Solids* **150** 35
[4] Tamura K, Hosokawa S, Inui M, Yao M, Endo H and Hoshino H 1992 *J. Non-Cryst. Solids* **150** 351
[5] Hoshino H, Miyanaga T, Ikemoto H, Hosokawa S and Endo H 1996 *J. Non-Cryst. Solids* **205–207** 43
[6] Endo H, Tamura K and Yao M 1987 *Can. J. Phys.* **65** 266
[7] Renninger A L and Averbach B L 1973 *Acta Crystallogr.* B **29** 1583
[8] Carron G J 1963 *Acta Crystallogr.* **16** 338
[9] Ma Q, Raoux D and Benezath S 1993 *Phys. Rev.* B **48** 16 332
[10] Cornet J and Rossier D 1973 *J. Non-Cryst. Solids* **12** 85
[11] Uemura O, Sagara Y, Tsushima M, Kamikawa T and Satow T 1979 *J. Non-Cryst. Solids* **33** 71
[12] Hosokawa S, Tamura K, Inui M and Endo H 1993 *J. Non-Cryst. Solids* **156–158** 712
[13] Hosokawa S, Sakaguchi F, Hiasa H and Tamura K 1991 *J. Phys.: Condens. Matter* **3** 6673
[14] Shimojo F, Munejiri S, Hoshino K and Zempo Y 1999 *J. Phys.: Condens. Matter* **11** L153
[15] Miyanaga T, Hoshino H, Ikemoto H, Yamamoto I and Endo H 1999 *Japan. J. Appl. Phys.* **38** 560
[16] Cabane B and Friedel J 1971 *J. Physique* **32** 73
[17] Enderby J E and Barnes A C 1990 *Rep. Prog. Phys.* **53** 85
[18] Kawakita Y, Yao M and Endo H 1999 *J. Non-Cryst. Solids* **250–252** 447
[19] Perron J C 1967 *Adv. Phys.* **16** 657
[20] Kawakita Y, Dong J, Tsuzuki T, Ohmasa Y, Yao M, Endo H, Hoshino H and Inui M 1993 *J. Non-Cryst. Solids* **156–158** 756
[21] Quinn R K 1974 *Mater. Res. Bull.* **9** 803
[22] Tsuzuki T, Yao M and Endo H 1995 *J. Phys. Soc. Japan* **64** 485
[23] Sakane H, Miyanaga T, Watanabe I, Matsubayashi N, Ikeda S and Yokoyama Y 1993 *Japan. J. Appl. Phys.* **32** 4641
[24] Rehr J J, Mustre de Leon J, Zabinsky S I and Albers R C 1991 *Phys. Rev.* B **44** 5135
[25] Hoshino H, Yamamoto I, Miyanaga T, Ikemoto H and Endo H 1999 *J. Non-Cryst. Solids* **250–252** 478
[26] Oberafo A A 1975 *J. Phys. C: Solid State Phys.* **8** 469
[27] Friedman L 1971 *J. Non-Cryst. Solids* **6** 329
[28] Nandakumar K and Philip J 1992 *J. Non-Cryst. Solids* **142** 247
[29] Hurst C H and Davis E A 1974 *J. Non-Cryst. Solids* **16** 343
[30] Tsuchiya Y 1999 *J. Non-Cryst. Solids* **250–252** 473
[31] Tsuchiya Y 1998 *Ber. Bunsenges.* **102** 1123
[32] Yao M, Suzuki K and Endo H 1980 *Solid State Commun. 34* 187
[33] Takimoto K and Endo H 1982 *Phys. Chem. Liq.* **12** 141
[34] Misawa M 1992 *J. Phys.: Condens. Matter* **4** 9491
[35] Cutler M, Kao S S and Silva L 1990 *Phys. Rev.* B **41** 3339
[36] Shimoi Y and Fukutome H 1992 *Prog. Theor. Phys.* **87** 307